

# *The Role of Near-Shore Bathymetry During Tsunami Inundation in a Reef Island Setting: A Case Study of Tutuila Island*

**Derya I. Dilmen, Gerard H. Roe, Yong  
Wei & Vasily V. Titov**

**Pure and Applied Geophysics**  
pageoph

ISSN 0033-4553

Pure Appl. Geophys.  
DOI 10.1007/s00024-018-1769-1



pure and  
applied  
geophysics

Vol. 170  
Nos. 9–10  
pp. 1361–1672  
2013  
ISSN 0033-4553

Special Issue:  
Historical and Recent  
Catastrophic Tsunamis in  
the World  
Vol. II - Tsunamis from 1755 to 2010

Editors:  
Kenji Satake  
Alexander B. Rabinovich  
Dale Dominey-Howes  
José C. Borrero

pageoph

 Birkhäuser

 Springer

**Your article is protected by copyright and all rights are held exclusively by This is a U.S. government work and its text is not subject to copyright protection in the United States; however, its text may be subject to foreign copyright protection. This e-offprint is for personal use only and shall not be self-archived in electronic repositories. If you wish to self-archive your article, please use the accepted manuscript version for posting on your own website. You may further deposit the accepted manuscript version in any repository, provided it is only made publicly available 12 months after official publication or later and provided acknowledgement is given to the original source of publication and a link is inserted to the published article on Springer's website. The link must be accompanied by the following text: "The final publication is available at [link.springer.com](http://link.springer.com)".**



## The Role of Near-Shore Bathymetry During Tsunami Inundation in a Reef Island Setting: A Case Study of Tutuila Island

DERYA I. DILMEN,<sup>1,2</sup>  GERARD H. ROE,<sup>2</sup> YONG WEI,<sup>1</sup> and VASILY V. TITOV<sup>1,2</sup>

**Abstract**—On September 29, 2009 at 17:48 UTC, an  $M_w = 8.1$  earthquake in the Tonga Trench generated a tsunami that caused heavy damage across Samoa, American Samoa, and Tonga. One of the worst hits was the volcanic island of Tutuila in American Samoa. Tutuila has a typical tropical island bathymetry setting influenced by coral reefs, and so the event provided an opportunity to evaluate the relationship between tsunami dynamics and the bathymetry in that typical island environment. Previous work has come to differing conclusions regarding how coral reefs affect tsunami dynamics through their influence on bathymetry and dissipation. This study presents numerical simulations of this event with a focus on two main issues: first, how roughness variations affect tsunami run-up and whether different values of Manning's roughness parameter,  $n$ , improve the simulated run-up compared to observations; and second, how depth variations in the shelf bathymetry with coral reefs control run-up and inundation on the island coastlines they shield. We find that no single value of  $n$  provides a uniformly good match to all observations; and we find substantial bay-to-bay variations in the impact of varying  $n$ . The results suggest that there are aspects of tsunami wave dissipation which are not captured by a simplified drag formulation used in shallow-water waves model. The study also suggests that the primary impact of removing the near-shore bathymetry in coral reef environment is to reduce run-up, from which we conclude that, at least in this setting, the impact of the near-shore bathymetry is to increase run-up and inundation.

**Key words:** Tsunami, numerical modeling, manning roughness, island reef environment, American Samoa.

### 1. Introduction

A topic of longstanding interest in tsunami research is the role of near-shore bathymetry in

tsunami dynamics (Leschka et al. 2009a; Lynett 2016). One particularly important example is the complex tsunami dynamics occurring in reef environments. The impact of reef-related bathymetry in affecting the destructiveness of tsunamis on the coast has been studied numerically and experimentally. For example, a study on Tutuila Island by Roeber et al. (2010) concluded that shallow reefs, in some instances, provided little or no protection to the coastal communities, and even transformed waves into having more destructive power. Roeber et al. (2010) also observed that fringing reefs and small embayments can amplify near-shore energy and develop local oscillation modes with 2–4-min periods adjacent to the shore of Tutuila. Tsunami observations, suggesting little protection by the coral reefs at atolls and reef-surrounded islands, were reported in the literature for the Tohoku tsunami impacts (Ford et al. 2013; Titov et al. 2016). On the other hand, Baba et al. (2008) performed numerical simulations of the 2007 Solomon Islands tsunami to explore the effect of the Great Barrier Reef on tsunami wave height and found that, in the simulations in which the reef was removed, the tsunami amplitude was larger by a factor of two or more than that produced by the model with the reef. Gelfenbaum et al. (2011) performed numerical simulations of the 2009 Samoa tsunami and concluded that a better understanding of reef roughness in particular is required to predict how coral reefs affect tsunami inundation. Experimental and theoretical studies indicated that reefs have a strong bottom drag coefficient that is about an order of magnitude larger than that for sand (see, e.g., Baptista et al. 1998; Kraines et al. 1998). Motivated by those results, Kunkel et al. (2006) performed simple one-dimensional and two-dimensional

<sup>1</sup> NOAA Center for Tsunami Research, Pacific Marine Environmental Laboratory, UW/Joint Institute for the Study of the Atmosphere and Ocean, 7600 Sand Point Way NE, Bldg. 3, Seattle, WA 98155, USA. E-mail: Vasily.Titov@noaa.gov

<sup>2</sup> Department of Earth and Space Sciences, University of Washington, Seattle, WA 98195-1310, USA.

numerical simulations with idealized topography to explore the effect of bottom friction due to a reef on tsunami run-up. With bathymetry held constant, the tsunami run-up was decreased approximately 50% when the bottom-drag coefficient was increased from 0.03 to 0.1. However, the Kunkel et al. (2006) simulations also suggest the possibility that gaps between adjacent reefs can result in flow amplification and actually increase the local wave heights. Fujima (2006) suggest that the increased damage observed at some islands in Maldives resulted from the tsunami front becoming more bore-shaped as it propagated over the fringing reef, which increased the destructive force of the wave. Fernando et al. (2005) and (2008) lend support to these numerical results: coral reefs protect coastlines behind them but local absences of reefs cause local flow amplification due to gaps. Their results are based on field observations, laboratory measurements (Fernando et al. 2008), and interviews of local people in Sri Lanka after the 2004 Indian Ocean tsunami. However, their laboratory simulations treated corals as a submerged porous barrier made of a uniform array of rods, which likely oversimplifies the complex structural distribution of coral reefs. Liu et al. (2009) found that wave amplitudes can be amplified several-fold (up to tenfold), based on the near-shore bathymetry.

In this study, we extend the analysis of reef roughness and reef bathymetry to a slightly more general study of the influence of reef-related bathymetry on tsunami impact, with a numerical-model case study of the 2009 Samoa tsunami on Tutuila island. We focus on two main goals: firstly, we want to understand how roughness variations of the shelf around the island affect run-up and inundation; secondly, we perform a model sensitivity analysis varying the bathymetry where fringing coral reefs exist, to elucidate the role of such reef-island bathymetry in controlling run-up on the coastlines it shields. For this event, localized run-up exceeded 17 m, and the event was well monitored by coastal tide gauges and off-shore DART buoys and post-tsunami run-up surveys.

The tsunami field surveys of 29 September 2009 Samoa tsunami on Tutuila Island showed that the western side of the island facing the tsunami direction had the highest wave run-up although with large

variations among adjacent villages only 2–3 km apart from each other; severe destruction was also apparent along the eastern and northern coastline of the island (Okal et al. 2010; Fritz et al. 2011; Borrero et al. 2011). It has proven difficult for numerical simulations of this event to successfully reproduce these large variations in tsunami run-up and inundation at many coastal villages (e.g., Dilmen et al. 2015). One challenge for numerical tsunami models in tropical settings such as this is to properly simulate the impact of the bathymetry including the pervasive barrier and fringing coral reefs (Fig. 1). In many respects, the 2009 Samoa tsunami provides an important benchmark for numerical models to simulate the tsunami dynamics in a typical submarine environment of coral-reef islands, with the ultimate goal of better understanding the tsunami risks for island communities around the world.

Our previous work (Dilmen et al. 2015) compared a tsunami simulation of this event with several observational datasets to evaluate the high variability of the tsunami impact around the Island of Tutuila. We found that the numerical model compares very well with tide gauge data. At the same time, the modeling of the inundation process clearly demonstrated the challenges for models in handling the complex bathymetric environment of coral islands. While the numerical simulation qualitatively reproduced inundation at all bays where flooding was observed, the quantitative comparison showed a tendency for the model to underestimate field-measured run-up values. We also found that there was a high degree of variability in the simulated run-up accuracy even among adjacent bays. Such model inconsistency and the measured run-up variability could not be explained by the presence of fringing reefs, nor did it correlate well with the available coral-reef damage data. There was only a tentative indication that at villages where the model underestimates run-up, coral damage is more likely to be high or very high, suggesting that the shallow-water models may overestimate energy dissipation over coral reefs.

The results implied that a more detailed understanding of two important model controls, roughness and bathymetry, would be a very useful next step in understanding the impact of reef-driven bathymetry on tsunami dynamics. Dilmen et al. (2015) also

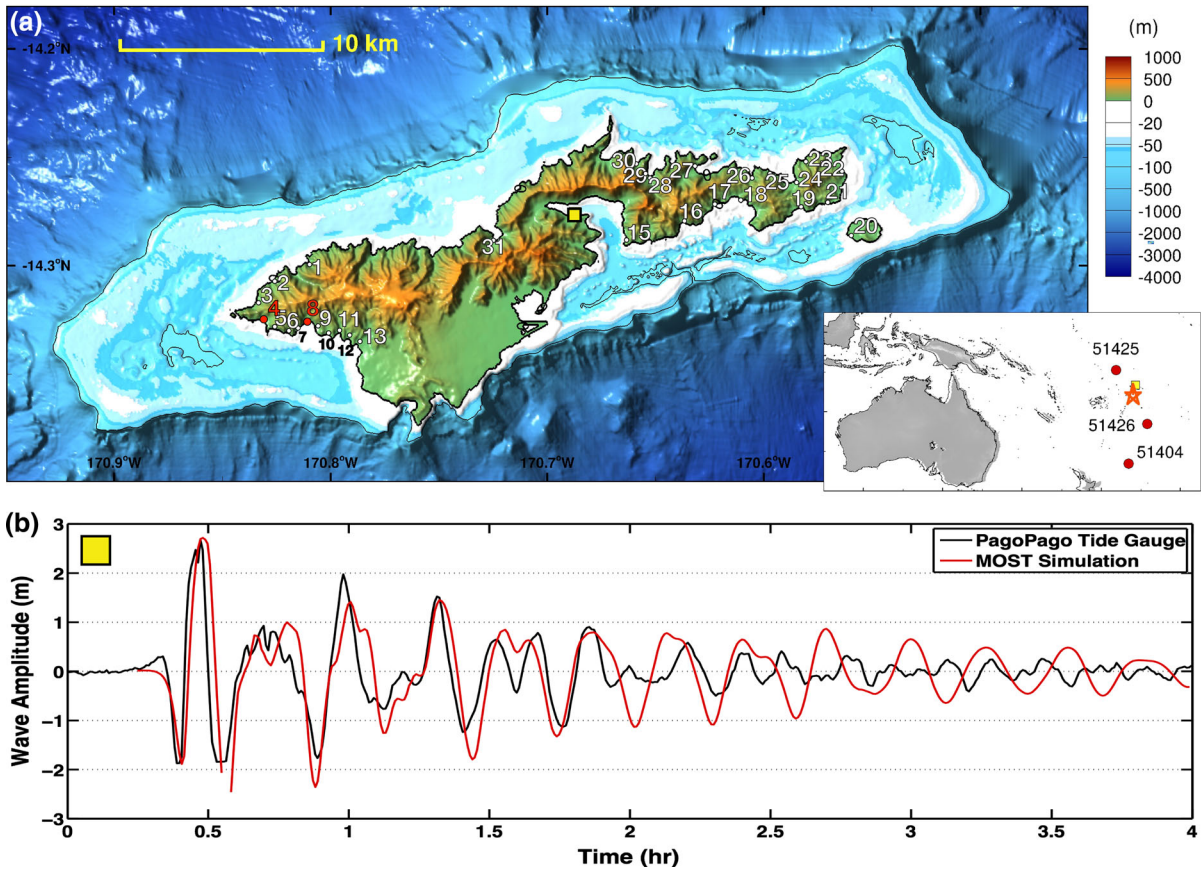


Figure 1

**a** Tutuila Island bathymetry. The numbers correspond to the locations of villages at which surveys were conducted, the yellow square is the location of the PagoPago tide gauge, locations of Amanave and Se'taga are indicated in red. Black lines show the coastlines and 90 m depth contour. Inset overview map: Tutuila Island tide gauge is shown as the yellow square. Red star shows the epicenter of the 2009 Samoa Earthquake; and the red circles are the location of the DART buoys used in optimizing the earthquake fault source used in the MOST simulations. **b** A comparison of the measured and simulated tsunami time series at the Pago Pago gauge location

evaluated the relationship between the tsunami dynamics and the coral damage by numerical modeling and post-tsunami surveys. They speculated that the variability in simulated run-up differences in the high-resolution tsunami model might be due to sharp changes in bottom roughness values caused by coral reefs. One expects that in reality there are strong spatial variations in roughness values (e.g., Nunes and Pawlak 2008). It is possible then that a different roughness coefficient used in a numerical simulation might more accurately simulate the run-up. The numerical model used for these simulations employs shallow-water equations, which is the classic modeling technique used in tsunami hazard assessment

and forecast. Because these equations are developed using the assumption that the velocity distribution is uniform in the vertical direction, it is unlikely those equations can adequately reproduce the complicated flows where the water depth suddenly changes near such reefs. Furthermore, the model represents dissipation using a parameterized bulk-drag formula (Eq. 1), with a single value for the Manning roughness coefficient, an empirically derived value taken from the engineering literature. Even though Dilmen et al. (2015) used a very high-resolution model for the Tutuila tsunami, there are significant differences between the observed and the modeled run-up and inundation; thus, modeling the flooding associated

with this event remains a challenge. Motivated by these issues, the present study focuses on two main goals: firstly, we want to understand how roughness variations affect run-up; secondly, we perform a model sensitivity analysis by varying the bathymetry where coral reefs exist, to elucidate their role in controlling run-up on the coastlines they shield.

The remainder of the paper is organized as follows: Sect. 2 summarizes the earthquake and tsunami event; Sect. 3 presents the modeling studies and the analyses; and Sect. 4 is the summary and discussion.

## 2. Model Description

We simulate the 2009 Samoa tsunami using the MOST Model (Titov 1997; Titov and González 1997; Titov et al. 2016). The evaluation of the simulations, a comparison with tide gauge and offshore DART data, and the calibration of the earthquake source function were described in Dilmen et al. (2015). MOST is an established tsunami model that has been widely tested and evaluated, and it is used operationally for forecasting (e.g., Titov 2009; Titov et al. 2016) and hazard assessment (e.g., Titov et al. 2003a). There are other numerical tsunami models with alternative dynamical equations and/or numerical schemes. Recognizing the importance for inter-model evaluations (e.g., Synolakis et al. 2008), recent community efforts have focused on using models that satisfy theoretical benchmarks and case-study comparisons, such as those proposed by the National Tsunami Hazard Mitigation Program (NTHMP 2012). MOST meets the benchmarks and performs comparably to other tsunami models for the real-world case studies. The primary metrics for comparison with observations are wave run-up, inundation from post tsunami surveys at 31 villages around Tutuila, and tide-gauge data (Fig. 1).

Dilmen et al. (2015) described in detail the numerical-model setup, earthquake source, and comparison of model results with observations. A set of three, nested computational grids that zoom into the simulation area are defined around Tutuila, with successively finer spatial resolution (A-grid is outermost coarse grid, B-grid is intermediate, and C is the innermost fine-scale grid). Details of the grid resolution are listed in Table 1.

Regional bathymetry and topography datasets were compiled and provided by National Center for Environmental Information (NCEI).

## 3. Analysis

### 3.1. The Impact of Changing Manning's Roughness, $n$

In the MOST numerical model, the effects of bottom friction are implemented by incorporating a basal shear stress with components  $(\tau_{xz}, \tau_{yz})$  into the shallow water equations and parametrized by a drag formula:

$$(\tau_{xz}, \tau_{yz})/\rho = -C_B \frac{\sqrt{U^2 + V^2}}{D} (U, V), \quad (1)$$

where  $U, V$  are the components of the velocities,  $D$  is the fluid depth, and  $\rho$  is the density (Titov et al. 2003b).  $C_B$  is the dimensionless friction coefficient, which can in turn be related to the Manning's roughness parameter,  $n$ , via:

$$C_B = \frac{gn^2}{D^{1/3}}. \quad (2)$$

The concept of Manning's roughness was originally developed for open-channel flow. Manning's  $n$  values have been measured empirically for a wide variety of different materials in laboratory experiments (Chow 1959), and by large-scale field studies of river flow for fully turbulent conditions (Bricker et al. 2015). From Eq. (1),  $C_B$  is depth-dependent, with increasing depth implying decreased friction. For example, for  $n = 0.025 \text{ s m}^{-1/3}$ ,  $C_B = 0.006$  for  $D = 1 \text{ m}$ , but  $C_B = 0.0025$  for  $D = 15 \text{ m}$ . Bottom friction typically has the greatest impact at depths of 0–10 m, and is negligible for tsunami propagation in the deep ocean (Levin and Nosov 2016). The simple

Table 1

Computational grids for simulations

Parameters	Grid A	Grid B	Grid C
Resolution	12 arc sec (360 m)	2 arc sec (60 m)	0.3 arc sec (10 m)
Size	1110 × 781	900 × 396	2400 × 2000

form of  $n$ , its relatively straightforward implementation within shallow-water equations, and the availability of extensive datasets of experimentally verified values, have led to its widespread adoption in tsunami modeling (e.g., Imamura et al. 2008) for the representation of frictional dissipation of tsunami energy in coastal zones, for both the submerged and subaerial portions of the domain. In many studies, a value of  $n = 0.025 \text{ s m}^{-1/3}$  has been adopted as appropriate for a smooth sea bottom or land. A range of other values has also been suggested from  $n \sim 0.01$  to  $0.1 \text{ s m}^{-1/3}$  depending on the setting and basal conditions (Kunkel et al. 2006; Tang et al. 2009; Jaffe et al. 2010; Gelfenbaum et al. 2011; and Bricker et al. 2015).

In our previous study of the 2009 Samoa tsunami on Tutuila island (Dilmen et al. 2015), we selected  $n = 0.03 \text{ s m}^{-1/3}$ . Both far-field pressure sensors (DARTs) and near-field coastal sea-level stations (tide gauges) were used to calibrate the tsunami source for this event. Simulated wave amplitudes matched well with tide-gauge observations (Fig. 1). Inundation computations from the model have been compared with point data of field run-up measurements. While the model confirmed and reproduced inundation at all 31 flooded villages, the comparison of simulated values with point observations revealed that the model underestimates the run-up at 15 village sites for this event, especially at sites behind heavily damaged coral reefs. Dilmen et al. (2015) implied that the model may have overestimated the energy dissipation over corals, possibly due to improper model roughness.

In this study, we first evaluate whether a different value of  $n$  can decrease the discrepancy between simulated and observed run-up at the 31 villages. For some villages, several separate run-up observations were made. For such villages, we took the average of all run-up observations. From the model output, we took the maximum simulated run-ups in a  $3 \times 3$  grid box ( $30 \text{ m} \times 30 \text{ m}$ ) surrounding the locations of each of the observations, and averaged them. We also tried taking just the maximum simulated run-up in the  $3 \times 3$  grid box, and comparing this with the maximum run-up observations at that village. Finally, we tried taking the maximum simulated run-up from the single gridpoint overlaying each run-up observation.

Our results do not depend on which of these various methods we use.

We performed simulations varying  $n$  from 0.01 to  $0.15 \text{ s m}^{-1/3}$ , where the lowest  $n$  value represents an essentially smooth bathymetry over the reef. In Fig. 2 we present the simulations for varying  $n$  as a scatterplot of observed vs. simulated runup at 31 villages around Tutuila. The locations of the villages are shown in Fig. 1. A comprehensive summary of the data and analyses is presented in Table 2 in Appendix.

Overall, for most of the villages, the variation of runup with  $n$  is straightforward, with higher values of  $n$  having less run-up. For some villages, however, the relationship is not monotonic, and the highest simulated runup does not always occur for the lowest value of  $n$ . Thus, at individual locations, the complex patterns of refraction and reflection, and nonlinear interactions can complicate the relationship between dissipation and runup. This is also clear from the different spreads among the simulated run-ups at individual villages. At some villages, there is very little spread in simulated runup as  $n$  varies (e.g., Fagatele village, observed runup = 4.92 m, the spread is 4% of the mean simulated value), whereas

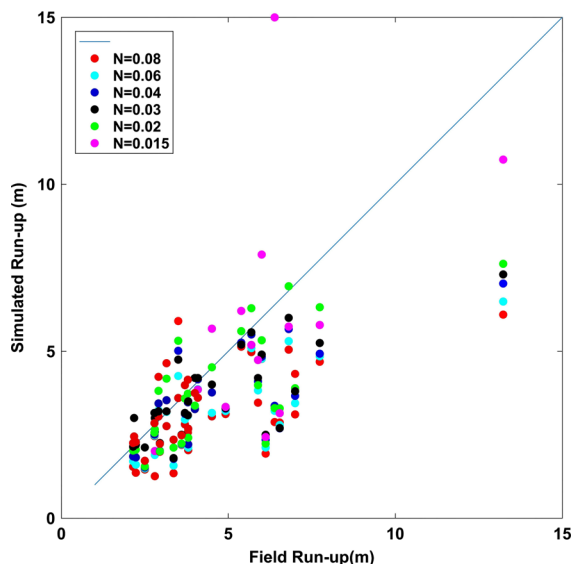


Figure 2

A comparison of model and field run-up for the simulations with varying  $n$  at 31 villages in Tutuila Island. The blue line shows the 1:1 line. Points falling on or close to the blue line show where there is good agreement between simulations and observations

at others the spread is large (e.g., Poloa village, observed runup = 13.5 m, the spread is 76% of the mean simulated value).

The results are mixed regarding whether the various values of  $n$  improve the simulated runup compared to observations. The model estimation of run-up is improved by changing  $n$  for some villages and doesn't change significantly at others. Of the total 31 villages, at 10 villages the difference between observed and estimated run-up is smallest when  $n = 0.02 \text{ s m}^{-1/3}$ . At 9 villages, the closest match occurs for  $n = 0.03 \text{ s m}^{-1/3}$ . At 5 villages, the closest match occurs for  $n = 0.015 \text{ s m}^{-1/3}$ . For the remaining 6 villages, two villages each achieve the closest match to observations when  $n = 0.04 \text{ s m}^{-1/3}$ ,  $n = 0.06 \text{ s m}^{-1/3}$ , and  $n = 0.08 \text{ s m}^{-1/3}$ .

In our simulations,  $n$  is uniform throughout the model domain, which oversimplifies the real situation of a heterogeneous littoral and coastal environment. Equations (1) and (2) represent dissipation in these environments. An obvious next step in tsunami modeling is to evaluate whether variations in basal conditions might be represented by spatial variability in  $n$ . Introducing spatial variations in  $n$  would add tunable degrees of freedom in the model, and in practical applications it would be important not to over-constrain a model. Nonetheless, an evaluation could be performed as to whether spatial variations in  $n$  might be optimized against observations to provide agreement with detailed measurements in case studies such as ours, and it would represent a 'best-case' for the ability of equations to simulate run up in these events. Since the computational influence of friction is strongest in the very near-shore and onshore environments (the influence is inversely proportional to flow depth), even a simplified uniform-friction study like ours can provide insight for the problem. Calibrating a variable-friction map for such a variable-friction simulation represents a formidable challenge. However, general hydrodynamic studies combined with measurements of wind- and tidal-driven currents in coral-reef lagoons (where the problem appears to be the most acute) can provide needed data for variable-friction maps and hence more precise estimates of the run-up and associated currents for shallow-water wave simulations.

Next, we evaluate the spatial patterns of the maximum tsunami amplitudes for two representative villages, Se'etaga and Amanave, as a function of  $n$ . Dilmen et al. (2015) showed that, for standard parameters ( $n = 0.03 \text{ s m}^{-1/3}$ ), our modeling successfully simulated the run-up observations at Se'etaga, agreeing to within 2.4%. On the other hand, just 3 km southeast from Se'etaga, the simulation did a relatively poor job for the village of Amanave (the model underestimated observed run-up by 45%). This very different simulation performance illustrates the complexities of the setting, and thus made Se'etaga and Amanave suitable for our case studies.

Figure 3 shows the tsunami evolution during the propagation toward the west coast of Tutuila Island where the two villages are located, for the simulation that provided the best fit with the tide-gauge record. These snapshots of the model amplitudes illustrate the dimensions and shape of the tsunami waves at the time of the initial flooding event at the two selected village locations. The figure shows that the wavelength of the tsunami in deep water is comparable with the size of Tutuila Island. However, when the wave reaches the shallow areas of the west-coast shelf, the wavelength shortens to approximately the length of the shelf. The wave exhibits strong refraction around the island due to the dramatic bathymetry changes near the island shelf. The strong amplification of the wave amplitude and shortening of the wavelength over the shelf lead to an increased steepness of the wave front, indicating mild to strong nonlinearity during the shoaling of the tsunami near the two selected locations.

The simulated maximum wave amplitude fields are shown in Fig. 4a–d for Se'etaga, and in Fig. 4e–h) for Amanave. For Se'etaga,  $n = 0.03 \text{ s m}^{-1/3}$  provides the best agreement in run-up (5.69 m observed, 5.57 m model), whereas for Amanave,  $n = 0.02 \text{ s m}^{-1/3}$  gives closest agreement (7.74 m observed, 6.32 m model). For higher values of  $n$ , the wave-amplitude fields vary smoothly on scales of few-hundred meters. The highest values of run-up are found in the center of both bays, suggesting a refraction or focusing of wave energy there. As  $n$  is reduced from 0.04 to  $0.02 \text{ s m}^{-1/3}$ , some significant localized increases in wave amplitude and inundation



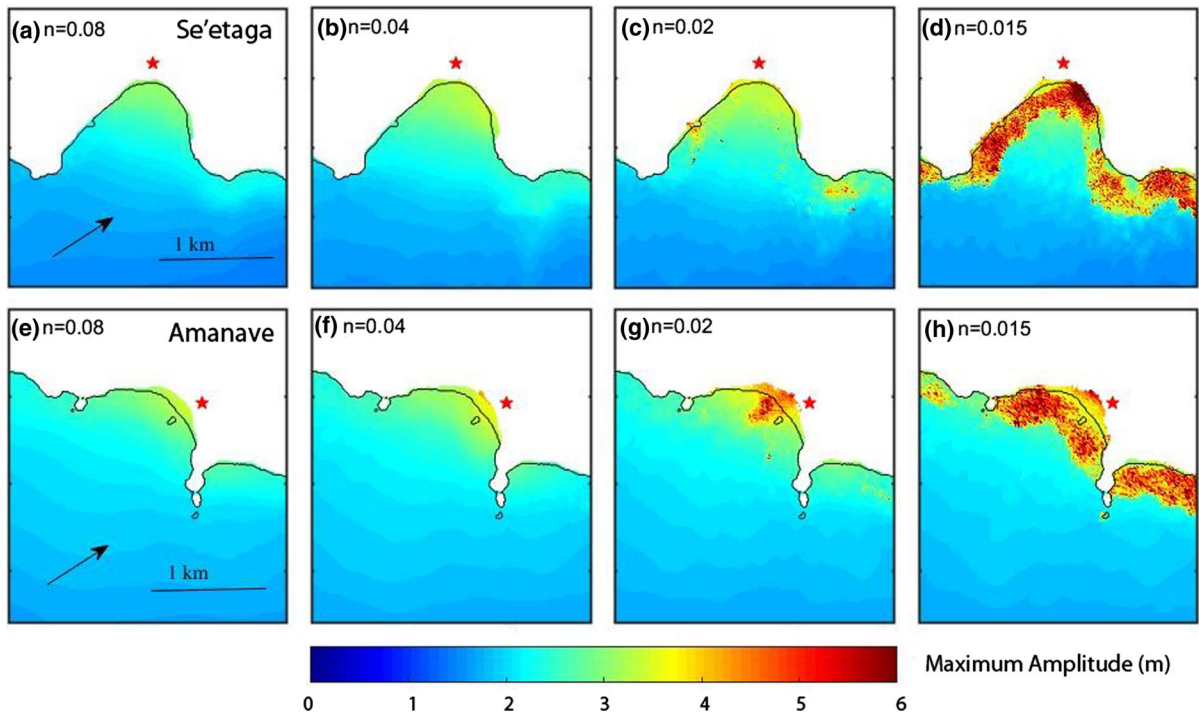


Figure 4

Simulated maximum wave amplitudes are shown for the bays near the villages of Se'etaga (top panels) and Amanave (lower panels) for  $n = 0.08, 0.04, 0.02$  and  $0.015 \text{ s}^{-1/3}$ . The pre-tsunami shoreline is shown as a thin black line. Colors inland of that line therefore show the degree of inundation. Village locations are shown as red stars. Black arrows indicate the tsunami direction from its source

by the shoreward-shoaling bathymetry. Note the middle panels also show that the lower values of  $n$  produce a larger momentum flux at offshore locations, showing that the greater dissipation associated with higher  $n$  is felt several km offshore. Finally, the bottom panels of Figs. 5 and 6 show the maximum computed bed shear stress from Eq. 3. It is noteworthy that the nearshore stresses are greater for lower values of  $n$ , despite the scaling in Eq. (3). The increased velocities outweigh the smaller  $n$  and larger  $D$  resulting in larger stresses. It is also clear that the largest stresses are associated with the individual reef structures seen in detail in Fig. 7b, c.

We next turn to a comparison of water-surface elevations at virtual sea-level gauges estimated from the MOST output at gridpoints near the coasts of Se'etaga and Amanave, for varying  $n$  (Fig. 7). At these villages, the maximum wave amplitude occurs during the first surge. For the Se'etaga time series, the maximum water elevations are 3.1, 3.2, and 3.3 m for

$n = 0.08, 0.04,$  and  $0.02 \text{ m s}^{-1/3}$ , respectively (Fig. 7). At Amanave, the maximum water elevations are 3.1, 3.4, and 3.9 m for  $n = 0.08, 0.04,$  and  $0.02 \text{ m s}^{-1/3}$ , respectively. The various values of  $n$  do not affect the timing of the waves, and have most impact on the amplitude of the first wave.

Both Se'etaga and Amanave time series show some evidence of resonance or constructive interference between approaching and receding waves (Fig. 7). We generally expect successive wave heights to decrease in amplitude after several waves, but at both sites wave elevations increase between the fourth and sixth waves then decrease again after the seventh wave. The time series at Se'etaga shows that the approaching and reflecting waves from the coastlines and bathymetry barriers form constructive interference after the third wave. Tsunami time series at Amanave drop off in amplitude more quickly than at Se'etaga and have a less sinusoidal form. By 1.5 h after the first waves, the tsunami has become a

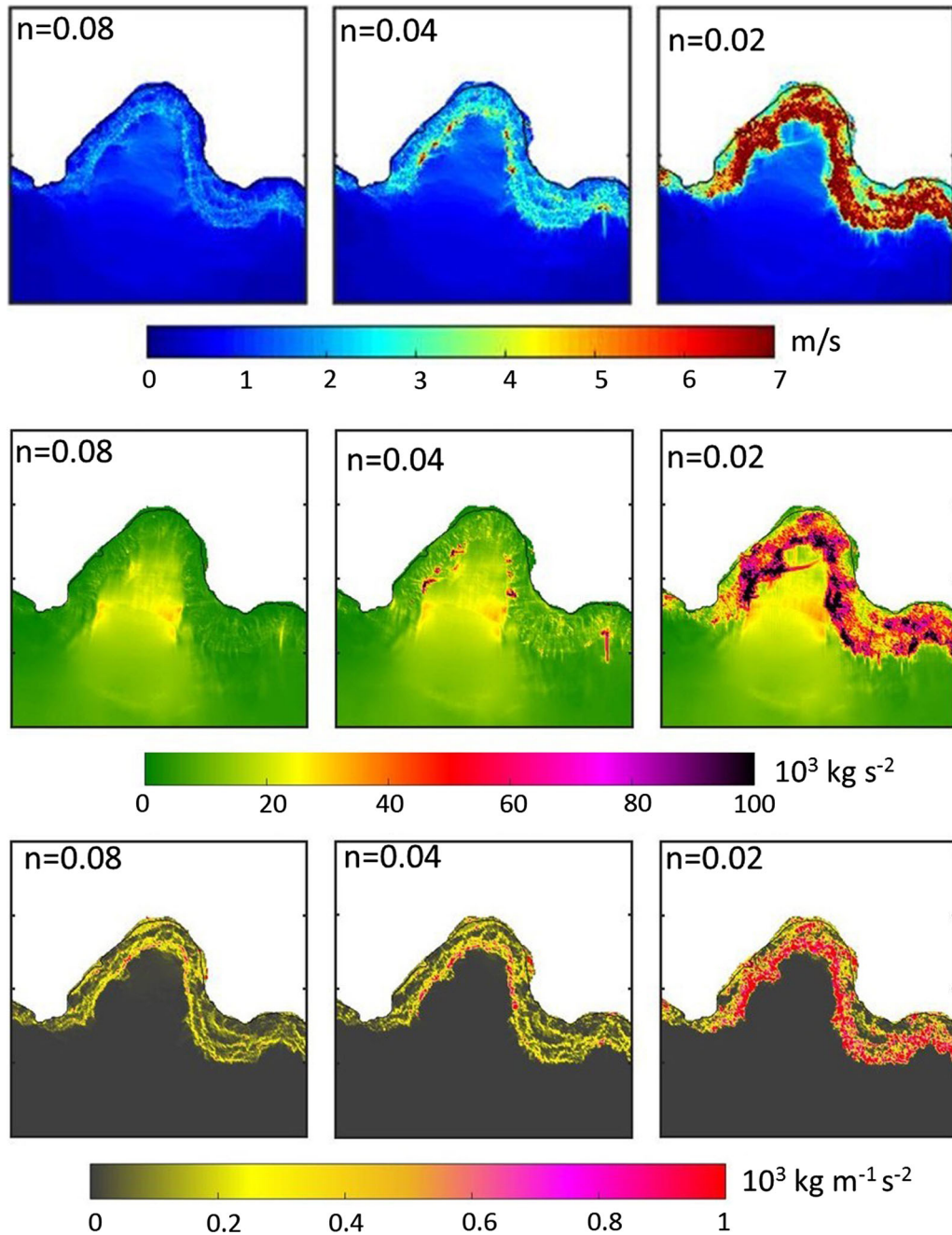


Figure 5

Dynamical fields from simulations for Se'etaga Bay as a function of Manning roughness,  $n$ . Upper panels: maximum flow velocity for  $n = 0.08, 0.04,$  and  $0.02 \text{ s m}^{-1/3}$ ; middle panels: maximum momentum flux for  $n = 0.08, 0.04,$  and  $0.02 \text{ s m}^{-1/3}$ ; bottom panels: maximum bed shear stress for  $n = 0.08, 0.04,$  and  $0.02 \text{ s m}^{-1/3}$ . The figure shows the maximum value of the field at every grid point, whenever it occurs in the model simulation. This accounts for the linear features seen in some of the panels

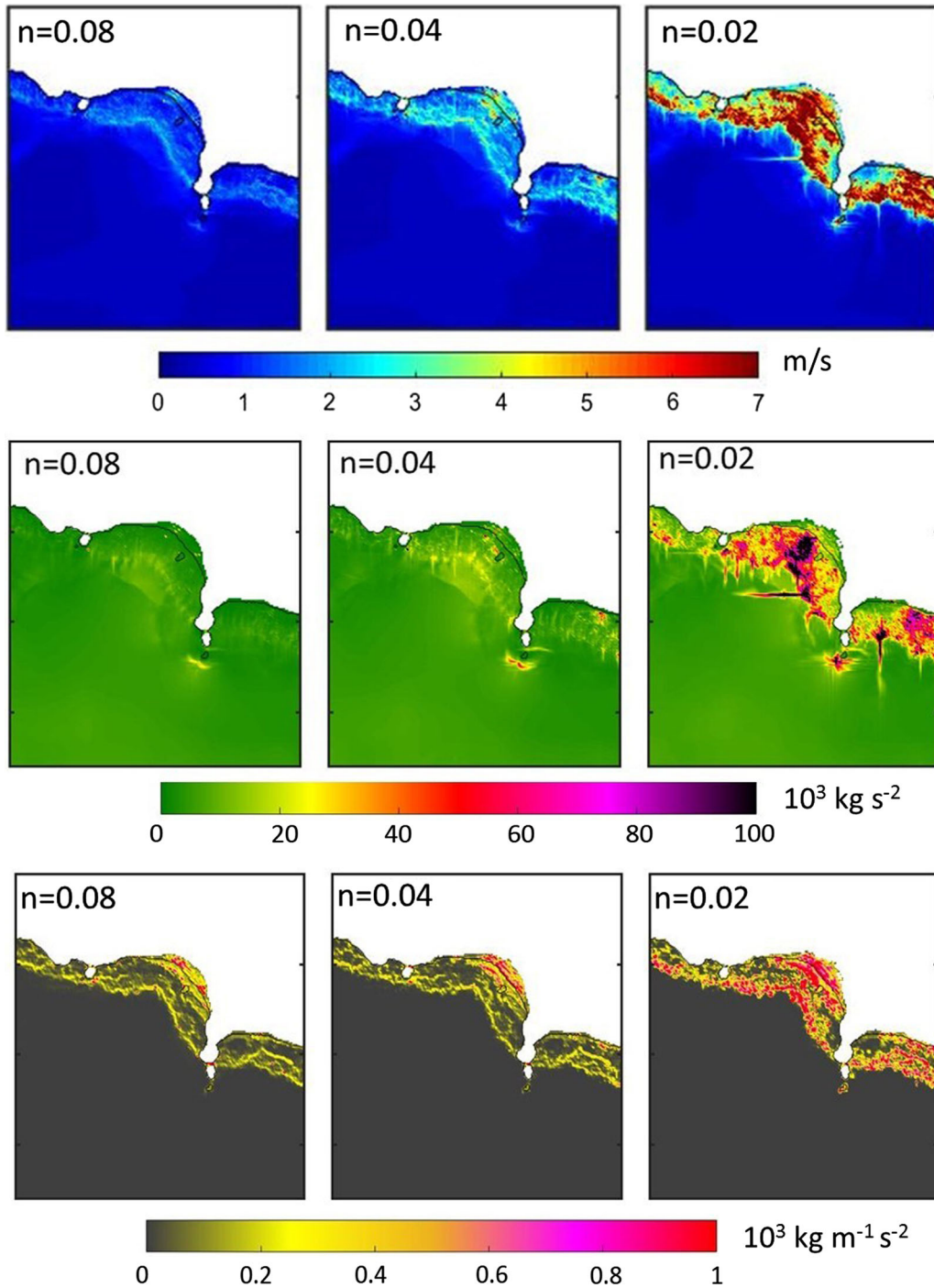


Figure 6  
As for Fig. 4, but for Amanave Bay

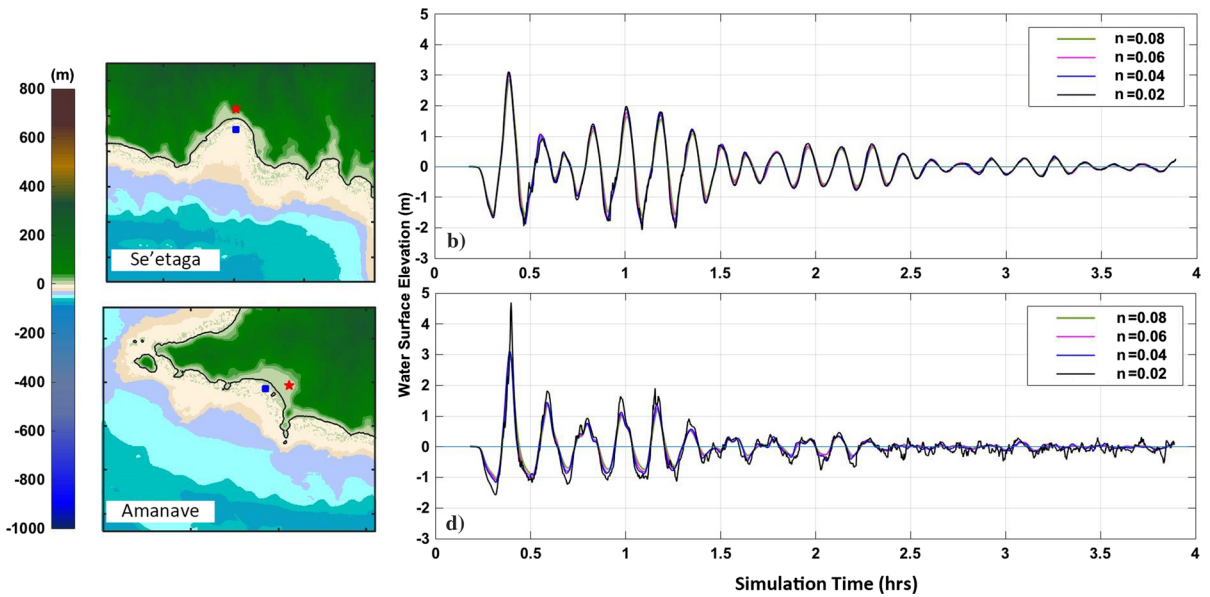


Figure 7

Comparison of water-surface elevations at selected virtual tide gauges in the near-shore regions of villages of Se'etaga (a, b) and Amanave (c, d). Maps show the location of the villages as red stars, and the locations of the virtual tide gauges are shown as blue squares. In b and d water surface elevations are given for varying  $n$  during the 4 h after the fault rupture at  $t = 0$

distorted noisy wave-train. This behavior indicates more nonlinearity and more overall dissipation, compared to Se'etaga, perhaps because of the more complicated reef structures within the bay that cause the waves to be dispersed in the reef areas (Fig. 7a compared with Fig. 7c).

### 3.2. Changes of Island Shelf Bathymetry

In this section, we evaluate how variations in island shelf bathymetry with the associated contributions from reef structures affect the tsunami run-up and inundation inside the bays at the 31 villages around Tutuila. We generate synthetic bathymetries for the higher-resolution grids of our nested computational grid system (the B and C grids of Table 1) by progressively removing bathymetry with less than 90 m depth (i.e., bathymetry in the range 0–90 m is ultimately set equal to 90 m). As shown in Fig. 1, the 90 m contour outlines the bathymetry inside the barrier reef. Therefore, such a procedure will gradually remove all reef-related bathymetry structures, including bathymetry features related to the fringing and barrier reefs, while leaving the flat 90 m-deep

shelf in front of the coastline intact. Let  $z_{\text{real}}(x, y)$  be the real bathymetry and let  $z_{\text{flat}}(x, y)$  be the extreme flattened bathymetry. We performed several experiments varying the bathymetry smoothly between these limits using the parameter,  $r$ , in the following equation:

$$z_{\text{expt}}(x, y) = rz_{\text{real}}(x, y) + (1 - r)z_{\text{flat}}(x, y) \quad (4)$$

Thus,  $r = 1$  corresponds to the real bathymetry and  $r = 0$  to the flattened bathymetry. We varied  $r$  from 0 to 1 in increments of 0.2. The resulting bathymetries are shown in Fig. 8. In all simulations, a value of Manning's roughness of  $n = 0.03 \text{ m s}^{-1/3}$  has been implemented.

We first focus on maximum wave amplitudes in simulations that implement these varying bathymetries. The wave amplitude fields near Se'etaga and Amanave are shown in Fig. 9, and the results for simulated run-up for villages around Tutuila are given in Table 3 in Appendix. In general, we find that wave amplitudes and run-up are smaller when the reef-related roughness of the original bathymetry is removed, contrary to the common belief that reefs and related bathymetric features protect reef-

surrounded coasts from tsunamis (Baba et al. 2008; Kunkel et al. 2006). When there is a smooth shelf ( $r = 0$ ), the tsunami run-up achieves its lowest value at 22 out of the 31 villages. For the remaining 9 villages, 4 villages achieve the smallest run-up when  $r = 0.2$ , 2 villages achieve the smallest run-up when  $r = 0.4$ , and 3 villages achieve the smallest run-up when  $r = 0.6$  (Table 3 in Appendix).

The same basic behavior is observed in the maximum wave amplitude fields near Se'etaga and Amanave (Fig. 9). Wave amplitudes are larger for the real bathymetry than for the flattened bathymetry. The model estimates the maximum water surface elevations at Se'etaga village as 3.2, 2.2, and 2.1 m for  $r = 1.0$ , 0.8, and  $r = 0.0$ , respectively. At Amanave, the maximum water surface elevations are 3.4, 2.8, 2.1 m for  $r = 1.0$ , 0.8, and 0.0, respectively.

These results may seem counterintuitive at first glance, since the removal of apparently protective structures over the island shelf actually decreases the run-up and inundation for the two considered locations. While there are fairly straightforward hydrodynamic explanations for the phenomenon, the

results dispute the popular misconception that any bathymetry barriers on a shelf, particularly the ones associated with barrier reef islands would provide additional protection against a tsunami. These results can only be fully explained by the nonlinear wave dynamics, since linear theory (as manifested by a Green's law, for example) would assume same amplification for waves coming from deeper water, regardless of bathymetry profile experienced along the way. The increased particle velocities of higher-amplitude waves, when amplified over reef structures, may contribute to higher run-up values. The effects of non-linear wave transformation over the reef environment appear to create more energetic flows toward the coastlines, leading to larger run-up. The inundation limits can be seen in Fig. 9 from the color shading that lies inland of the pre-tsunami shoreline. It is interesting to note that the inundation limits are not a strong function of the offshore bathymetry, despite the very large variations we have implemented. It suggests that the extent of inundation may be more sensitive to the coastal geometry and topography, and the immediate near-shore bathymetry. Indirect evidence of this finding has been

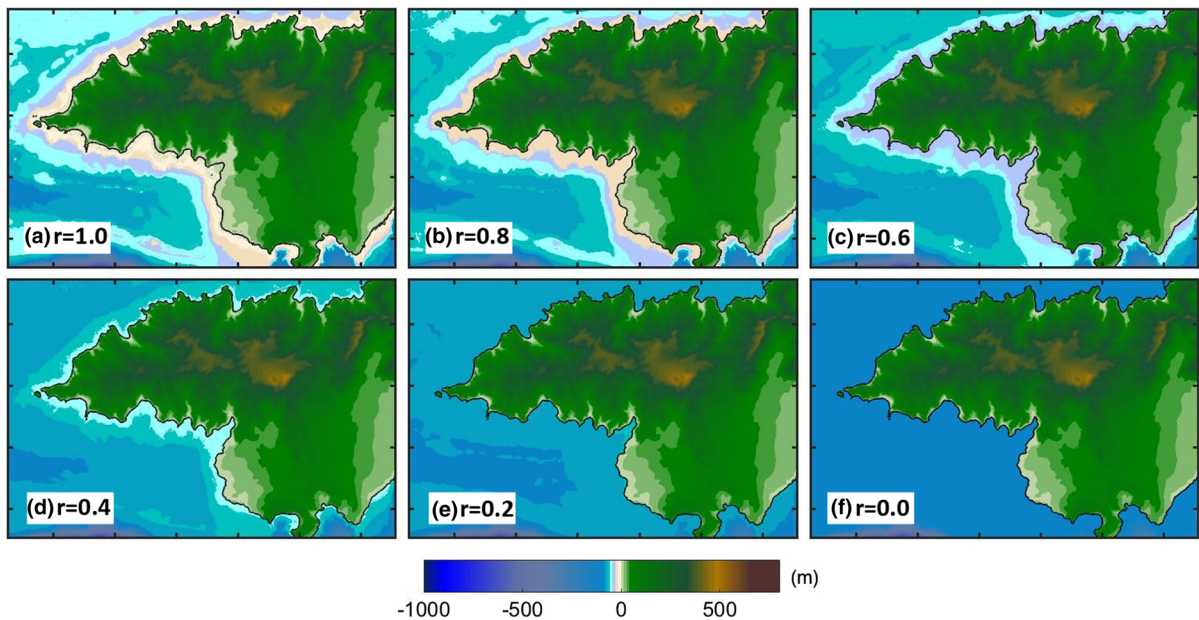


Figure 8

C grids of synthetic bathymetry generated from Eq. 3, shown for the west side of Tutuila Island.  $r = 1$  gives original bathymetry;  $r = 0$  gives flat shelf bathymetry from 0 m to 90 m depth

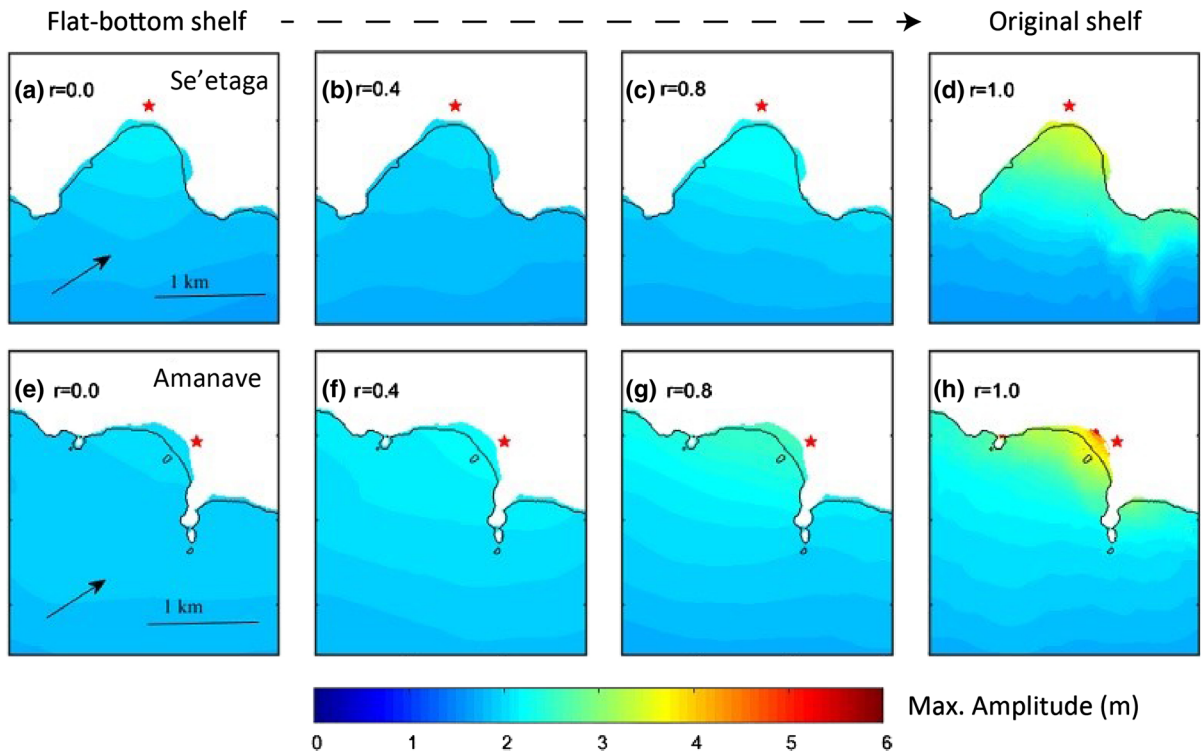


Figure 9

Simulated maximum wave amplitudes are shown for the bays near the villages of Se'etaga (top panels) and Amanave (bottom panel) for different bathymetry [ $r = 0.0$  (flat-shelf), 0.4, 0.8 and 1.0 (actual)]. The pre-tsunami shoreline is shown as a thin black line. Colors inland of that line therefore show the degree of inundation. Village locations are shown as red stars. Black arrows indicate tsunami direction

documented by Wei et al. (2013), who observed very consistent inundation area predictions with fairly high variability in amplitude comparisons. Thus, hi-res topographic data (such as from LiDAR surveys) are important for accurate inundation mapping.

Simulated time series computed at the same offshore locations near Se'etaga and Amanave villages provides additional illustration and some explanation for the decreased run-up without barrier reef- and fringing reef-related bathymetric structures (Fig. 10). In contrast to the results for varying roughness, changing the bathymetry prompted significant changes in the time series. As the bathymetry is progressively removed ( $r \rightarrow 0$ ), the first waves arrive 5–10 min earlier with generally smaller amplitudes and with shorter periods.

The time series show the significant influence of varying the bathymetry for the later tsunami waves in the two bays, due to wave resonance and shoaling. The resonance is particularly prominent in Se'etaga

bay (Fig. 9a). As the bathymetry is progressively removed ( $r \rightarrow 0$ ), the resonant amplification in the amplitude of waves 4–7 seen in Se'etaga Bay, diminishes and eventually disappears. Therefore, the resonant feature in the time series of the original bathymetry is probably related to the multiple reflections from the bathymetric features of the semi-enclosed lagoon inside the barrier reef, and not to coastal reflections. The time series also indicates that the run-up and inundation are mostly driven by the initial wave, which is the highest for all cases. Therefore, reflection and refraction are not playing significant role for the maximum run-up and inundation for the two locations. This is another indication that the nonlinear evolution of the wave over the shelf is predominantly responsible for the increased run-up for the original bathymetry.

Roeber et al. (2010) came to similar conclusion using resonant mode analysis of their numerical simulations for the 2009 Samoa tsunami around

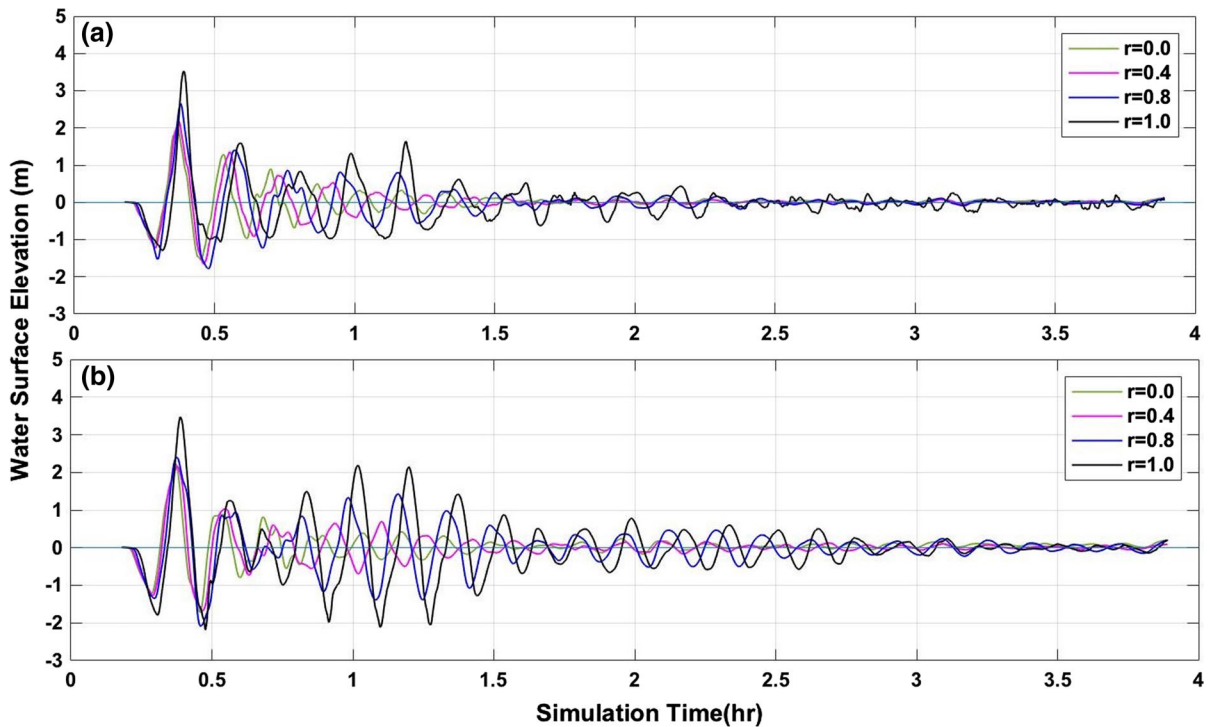


Figure 10

Comparison of water surface elevations at selected virtual tide gauges in the near-shore regions of villages of Se'etaga and Amanave. Refer to Fig. 7 for location of gauges. Water surface elevations are given for varying  $r$  in the 4 h after the fault rupture at  $t = 0$

Tutuila. They found significant resonant amplifications for relatively shorter wave periods at the west coast of Tutuila, where shallow reefs provided little protection for coastal population. Our work indicates that the reef-related bathymetric structures actually increase the run-up and, therefore, tsunami impact for coastal communities there.

#### 4. Discussion and Conclusion

Manning roughness,  $n$ , was spatially uniform in our simulations. Although almost all numerical codes can accommodate variable roughness, the use of a uniform roughness coefficient is standard practice in most current tsunami models. The main reason is the difficulty of determining the correct pattern of roughness values within the computational area. Also, the use of a lower roughness coefficient is thought to produce more conservative results (our study confirmed and quantified that notion), which is

desirable for many tsunami studies. Arguably, the uniform roughness is only valid at large scales, and cannot capture the real situation of a heterogeneous reef environment. An important frontier in tsunami modeling research is whether, in pursuit of more accurate predictions, models should incorporate spatially varying  $n$  or whether, in addition, the mathematical representation of the dissipation (Eqs. 1, 2) must be reformulated.

When we remove reef-related bathymetry structures, the modelled run-up values on the coast decrease, due to non-linear wave transformation over the reef flats. A notable feature of the simulations is that varying the bathymetry has a strong impact on the wave resonance that was observed. The bathymetry plays a significant role in the constructive interference of reflected and incident waves. As the bathymetry is progressively removed, the first waves arrive earlier and the period of successive waves gets longer, consistent with faster velocities in deeper water. Interestingly, similar dynamics were noticed

by Lynett (2007) for a set of one-dimensional numerical experiments with artificial bathymetry simulating the barrier and fringing reef environment. Lynett's numerical experiments showed peculiar increase of overland velocities when long obstacles were added to the one-dimensional bathymetry for weakly nonlinear waves, but not for highly nonlinear (very high amplitude) waves. While the geometry of these idealized one-dimensional experiments are different from our realistic 2-d modeling setting, the general dimensionless parameters of the 2009 Samoa tsunami wave are similar to the weakly nonlinear case of Lynett's simulations (Fig. 2). Our numerical results appear to confirm that such amplifications, wherein the reef shelf features increase the run-up, can occur in natural settings of reef islands like Tutuila. The dataset synthesized in Tables 2 and 3 in Appendix are summaries of the model results.

The role of reefs and reef-island shelf bathymetry in tsunami dynamics remains enigmatic, which echoes Lynett's (2016) conclusions about the chaotic nature of flow over complex bathymetries, and the resultant challenges inherent to the deterministic modeling of such flows. Our results add to a body of literature exploring this important question. In our experiments, the reef-related bathymetry enhanced run up via nonlinear tsunami transformation over reef structures. We designed our experiments to pervasively smooth and remove the reef-related small-scale bathymetry of the island shelf, rather than focusing on individual structures. To some degree, our results must depend on the proximity of the reefs to the shore. Broader reefs further from shore, such as the Great Barrier Reef example for instance, might dissipate wave energy enough to reduce onshore run up. However, given the degree of complexity we found in our simulations, it would be hazardous to conclude that reefs, and the reef-island bathymetric environment in general, provide universal protection for their inshore coastlines.

To conclude, while the impact of coral reefs on the dynamics of tsunamis impinging on tropical islands is obviously complicated and depends on many factors, our results reinforce a focus on two key issues that call for further research: first, the representation of the turbulent dissipation in terms of the governing equations and their coefficients; and second, the role of all aspects of reef-island bathymetry such as reef widths, reef types and coastal geometry on the scale of individual bays.

### *Acknowledgements*

This publication makes use of data products provided by National Oceanic and Atmospheric Administration (NOAA), Pacific Marine Environmental Laboratory (Contribution number 4618). This publication is partially funded by the Joint Institute for the Study of the Atmosphere and Ocean (JISAO) under NOAA Cooperative Agreement NA15OAR4320063, Contribution No. 2018-0131. Hermann Fritz generously provided the post-tsunami run-up survey datasets. We are grateful to Randall Leveque, Joanne Bourgeois, Frank Gonzales, Hongqiang Zhou, Christopher Moore, Marie Eble, Diego Arcas, Lijuan Tang, Jose Borrero and the anonymous reviewer for their endless advice and help.

### *Appendix*

These tables present MOST model output for maximum amplitude along selected villages (Fig. 1 for locations of the villages). There is a tendency that run-up increases with decreasing Manning coefficient and the model better estimates run-up (Table 2). There is also a tendency that run-up decreases with removing reefs (Table 3).

Table 2

*Model, simulated run-up (m) for different Manning's roughness, n, values at 31 villages around Tutuila*

Village # (Fig. 1)	Village name	Run-up field	Run-up, $n = 0.08$	Run-up, $n = 0.06$	Run-up, $n = 0.04$	Run-up, $n = 0.03$	Run-up, $n = 0.02$	Run-up, $n = 0.015$
31	LAUILI	3.36	1.35	1.58	1.78	1.80	2.12	2.35
30	AMALAU	2.50	1.46	1.49	1.52	2.12	1.55	1.72
29	AFONO1	2.18	1.92	1.98	2.06	3.00	2.20	2.45
28	AFONO2	3.80	2.04	2.11	2.21	3.50	2.41	2.68
16	AVAIO	3.70	2.81	2.95	3.12	3.15	3.59	3.98
27	MASEFAU	4.00	3.32	3.30	3.27	4.20	3.37	3.74
18	AMAU	2.91	3.05	3.23	3.43	3.20	3.81	4.23
17	FAGAITUA	3.50	3.60	4.26	5.02	4.75	5.31	5.90
26	MASAU	2.79	2.46	2.48	2.50	3.15	2.56	2.84
25	SAILELE	2.95	1.99	2.01	2.01	2.25	2.00	2.23
24	AOA	2.23	1.36	1.60	1.82	2.20	2.05	2.28
19	AMOU	3.15	2.76	3.18	3.53	3.20	4.18	4.64
23	ONENO	3.60	2.20	2.21	2.23	2.50	2.24	2.48
21	AUASI	3.79	2.57	3.06	3.47	3.08	3.73	4.14
22	TULA	7.00	3.11	3.44	3.66	3.80	3.89	4.32
20	AUNU	2.15	1.54	1.71	1.85	2.14	2.03	2.25
3	POLO	13.23	6.10	6.49	7.03	7.30	7.62	10.74
4	AMANAVE	7.74	4.69	4.85	4.93	5.25	6.32	5.79
2	FAGAILI	6.00	4.77	4.78	4.84	4.90	5.33	7.90
5	FAILOLO	6.54	2.87	2.79	2.69	2.70	3.29	3.14
6	AGUGULU	6.12	1.93	2.11	2.35	2.50	2.23	2.43
7	UTUMEA	4.51	3.05	3.15	3.76	4.00	4.52	5.68
8	SE'ETAGA	5.69	4.98	5.09	5.50	5.57	6.29	5.19
1	FAGAMALO	6.39	2.88	3.22	3.37	3.30	3.30	15.00
9	NUA	4.09	3.61	3.86	4.15	4.20	3.85	3.86
10	AFAO	5.89	3.46	3.83	4.10	4.20	3.98	4.74
11	ASILII	6.81	5.05	5.30	5.66	6.00	6.94	5.74
12	AMALUIA	5.39	5.14	5.26	5.26	5.20	5.60	6.21
13	LEONE	2.80	1.26	1.89	2.58	3.00	2.66	2.01
14	FAGATELE	4.92	3.12	3.21	3.28	3.30	3.33	3.33

## The Role of Near-Shore Bathymetry During Tsunami Inundation in a Reef Island Setting

Table 3

Model, simulated run-up for different  $r$  values representing varying bathymetry at 31 villages around Tutuila

Village # (Fig. 1)	Villages	Run-up field	Run-up, $r = 1$	Run-up, $r = 0.8$	Run-up, $r = 0.6$	Run-up, $r = 0.4$	Run-up, $r = 0.2$	Run-up, $r = 0.0$
31	LAULI	3.36	1.80	1.13	1.05	0.98	0.94	0.89
30	AMALAU	2.50	2.12	2.05	1.89	1.76	1.65	1.54
29	AFONO2	2.18	3.00	2.34	2.30	2.33	2.24	2.17
28	AFONO1	3.80	3.50	2.70	2.79	2.75	2.77	2.72
16	AVAIO	3.70	3.15	2.46	2.25	2.25	2.27	2.30
27	MASEFAU	4.00	4.20	2.80	2.49	2.58	2.61	2.70
18	AMAU	2.91	3.20	1.93	1.86	1.79	1.75	1.67
17	FAGAITUA	3.50	4.75	3.14	2.78	2.86	2.88	2.95
26	MASAUSI	2.79	3.15	2.15	2.10	1.99	1.95	1.98
25	SAILELE	2.95	2.25	1.55	1.63	1.47	1.49	1.43
24	AOA	2.23	2.20	1.90	1.76	1.72	1.69	1.63
19	AMOULI	3.15	3.20	3.67	2.87	2.93	2.87	2.80
23	ONENOA	3.60	2.50	1.69	1.41	1.42	1.40	1.33
21	AUASI	3.79	3.08	2.24	2.16	2.02	2.02	1.88
22	TULA	7.00	3.80	2.38	2.22	2.07	2.07	1.98
20	AUNUU	2.15	2.14	2.07	1.90	1.78	1.78	1.67
3	POLOA	13.23	7.30	5.32	5.12	4.79	4.46	4.14
4	AMANAVE	7.74	5.25	3.29	3.06	2.85	2.73	2.59
2	FAGAILII	6.00	4.90	4.75	4.36	4.08	3.82	3.56
5	FAILOLO	6.54	2.70	2.11	2.07	2.10	2.02	1.95
6	AGUGULU	6.12	2.50	1.93	1.99	1.96	1.98	1.94
7	UTUMEA	4.51	4.00	3.12	2.86	2.86	2.88	2.92
25	SE'ETAGA	5.69	5.57	3.71	3.30	3.43	3.46	3.59
1	FAGAMALO	6.39	3.30	1.99	1.92	1.84	1.81	1.72
9	NUA	4.09	4.20	2.78	2.46	2.53	2.54	2.17
10	AFAO	5.89	4.20	2.87	2.80	2.65	2.60	2.64
11	ASILII	6.81	6.00	4.14	4.34	3.91	3.96	3.83
12	AMALUIA	5.39	5.20	4.50	4.15	4.06	4.01	3.86
13	LEONE	2.80	3.00	3.44	2.69	2.75	2.69	2.62
14	FAGATELE	4.92	3.30	2.23	1.85	1.88	1.85	1.75

## REFERENCES

- Baba, T., Mleczo, R., Burbidge, D., Cummins, P. R., & Thio, H. K. (2008). The effect of the Great Barrier reef on the propagation of the 2007 Solomon islands tsunami recorded in Northeastern Australia. *Pure and Applied Geophysics*, 165(11), 2003–2018.
- Baptista, M. A., Miranda, P. M. A., Miranda, J. M., & Victor, L. M. (1998). Constrains on the source of the 1755 Lisbon tsunami inferred from numerical modelling of historical data. *Journal of Geodynamics*, 25, 159–174.
- Borrero, J. C., Greer, S. D., Lebreton, L., & Fritz, H. M. (2011). Field surveys and numerical modelling of the 2009 South Pacific and 2010 Mentawai Islands tsunamis. In *Proceedings of Coasts and Ports Conference*, Perth, Australia, September 28–30, 2011.
- Bricker, J. D., Gibson, S., Takagi, H., & Imamura, F. (2015). On the need for larger Manning's roughness coefficients in depth-integrated tsunami inundation models. *Coastal Engineering Journal*. <https://doi.org/10.1142/S0578563415500059>.
- Chow, V. T. (1959). *Open-channel hydraulics*. New York: McGraw-Hill Book Company.
- Dilmen, D. I., Titov, V. V., & Roe, H. G. (2015). Evaluation of the relationship between coral damage and tsunami dynamics; case study: 2009 Samoa tsunami. *Pure and Applied Geophysics*, 172(12), 3557–3572. <https://doi.org/10.1007/s00024-015-1158-y>.
- Fernando, H. J. S., McCulley, J. L., Mendis, S. G., & Perera, K. (2005). Coral poaching worsens tsunami destruction in Sri Lanka. *Eos Transactions American Geophysical Union*, 86(33), 301–304. <https://doi.org/10.1029/2005eo330002>.
- Fernando, H. J. S., Samarawickrama, S. P., Balasubramanian, S., Hettiarachchib, S. S. L., & Voropayeva, S. (2008). Effects of porous barriers such as coral reefs on coastal wave propagation. *Journal of Hydro-environment Research*, 1, 187–194.
- Ford, M., Becker, J. M., Merrifield, M. A., & Song, Y. T. (2013). Marshall Islands fringing reef and atoll lagoon observations of the Tohoku tsunami. *Pure and Applied Geophysics*. <https://doi.org/10.1007/s00024-013-0757-8>.
- Fritz, H. M., Borrero, J. C., Synolakis, C. E., Okal, E. A., Weiss, R., Titov, V., et al. (2011). Insights on the 2009 South Pacific tsunami in Samoa and Tonga from field surveys and numerical simulations. *Earth-Science Reviews*, 107, 66–75.
- Fujima, K. (2006). Effect of a submerged bay-mouth breakwater on tsunami behavior analyzed by 2D/3D hybrid model simulation. *Natural Hazards*, 39(2), 179–193.

- Gelfenbaum, G., Apotsos, A., Stevens, A. W., & Jaffe, B. (2011). Effects of fringing reefs on tsunami inundation: American Samoa. *Earth-Science Reviews*, *107*, 12–22.
- Imamura, F., Goto, K., & Ohkubo, S. (2008). A numerical model for the transport of a boulder by tsunami. *Journal of Geophysical Research*. <https://doi.org/10.1029/2007JC004170>.
- Jaffe, B. E., Gelfenbaum, G., Buckley, M. L., Steve, W., Apotsos, A., Stevens, A. W., & Richmond, B. M. (2010). The limit of inundation of the September 29, 2009, Tsunami on Tutuila, American Samoa: *U.S. Geological Survey Open File Report*, 2010–1018.
- Kraines, S. B., Yanagi, T., Isobe, M., & Komiyama, H. (1998). Wind-wave driven circulation on the coral reef at Bora Bay. *Miyako Island, Coral Reefs*, *17*, 133–143.
- Kunkel, M., Hallberg, R. W., & Oppenheimer, M. (2006). Coral reefs reduce tsunami impact in model simulations. *Geophysical Research Letters*. <https://doi.org/10.1029/2006GL027892>.
- Leschka, S., Kongko, W., & Larsen, O. (2009a). On the influence of nearshore bathymetry data quality on tsunami runup modeling, part I: Bathymetry. In *Proc. of the 5th International Conference on Asian and Pacific Coasts (APAC 2009)* (Vol. 1, pp. 151–156). Singapore: Soon Keat Tan, Zenhua Huang.
- Levin, B. W., & Nosov, M. A. (2016). Propagation of a tsunami in the ocean and its interaction with the coast. In Levin, B. W., & Nosov M. A. (Ed.), *Physics of tsunamis* (pp. 311–358). Springer. <https://doi.org/10.1007/978-3-319-24037-4>.
- Liu, P. L.-F., Wang, X., & Salisbury, A. J. (2009). Tsunami hazard and early warning system in South China Sea. *Journal of Asian Earth Sciences*, *36*(1), 2–12.
- Lynett, P. J. (2007). Effect of a shallow water obstruction on long wave runup and overland flow velocity. *Journal of Waterway, Port, Coastal, and Ocean Engineering*, *133*(6), 455–462. [https://doi.org/10.1061/\(ASCE\)0733-950X\(2007\)133:6\(455\)](https://doi.org/10.1061/(ASCE)0733-950X(2007)133:6(455)).
- Lynett, P. J. (2016). Precise prediction of coastal and overland flow dynamics: a grand challenge or a fool's errand. *Journal of Disaster Research*. <https://doi.org/10.20965/jdr.2016.p0615>.
- NTHMP, National Tsunami Hazard Mitigation Program. (2012). *Proceedings and Results of the 2011 NTHMP Model Benchmarking Workshop*. Boulder: U.S. Department of Commerce/NOAA/NTHMP, (NOAA Special Report), 436.
- Nunes, V., & Pawlak, G. (2008). Observations of bed roughness of a coral reef. *Journal of Coastal Research*, *24*(2B), 39–50.
- Okal, E. A., Fritz, H. M., Synolakis, C. E., Borrero, J. C., Weiss, R., Lynett, P. J., et al. (2010). Field survey of the Samoa tsunami of 29 September 2009. *Seismological Research Letters*, *81*(4), 577–591. <https://doi.org/10.1785/gssrl.81.4.577>.
- Roeber, V., Yamazaki, Y., & Cheung, K. F. (2010). Resonance and impact of the 2009 Samoa tsunami around Tutuila, American Samoa. *Geophysical Research Letters*. <https://doi.org/10.1029/2010GL044419>.
- Synolakis, C. E., Bernard, E. N., Titov, V. V., Kânoğlu, U., González, F. I. (2008). Validation and verification of tsunami numerical models. *Pure and Applied Geophysics*, *165* (11–12), 2197–2228.
- Tang, L., Titov, V. V., & Chamberlin, C. D. (2009). Development, testing, and applications of site-specific tsunami inundation models for real-time forecasting. *Journal of Geophysical Research*, *114*, C12025. <https://doi.org/10.1029/2009jc00547>.
- Titov, V. V. (1997). Numerical modeling of long wave runup, *PhD Thesis*, University of Southern California, p. 141.
- Titov, V. V. (2009). Tsunami forecasting. In A. N. Bernard & A. R. Robinson (Eds.), *The Sea. Tsunamis*, Chap. 12 (Vol. 15, pp. 371–400). Cambridge, MA: Harvard University Press.
- Titov, V., & González, F. I. (1997). Implementation and testing of the Method of Splitting Tsunami (MOST) model. *NOAA Tech. Memo. ERL PMEL-112 (PB98-122773)*, NOAA/Pacific Marine Environmental Laboratory, Seattle, WA, p. 11.
- Titov, V. V., Gonzales, F. I., Bernard, E. N., Eble, M. C., Mofjeld, H. O., Newman, J. C., et al. (2003a). Real-time tsunami forecasting: Challenges and solutions. *Natural Hazards*, *35*(1), 35–41.
- Titov, V.V., Gonzalez, F. I., Mofjeld, H. O., & Venturato, A. J. (2003b). NOAA TIME Seattle tsunami mapping project: Procedures, data sources, and products. *NOAA Tech. Memo. OAR PMEL-124, NTIS: PB2004-101635*, p. 21.
- Titov, V. V., Kânoğlu, U., & Synolakis, C. (2016). Development of MOST for real-time tsunami forecasting. *Journal of Waterway, Port, Coastal, and Ocean Engineering*, *142*(6), 03116004. [https://doi.org/10.1061/\(asce\)ww.1943-5460.0000357](https://doi.org/10.1061/(asce)ww.1943-5460.0000357).
- Wei, Y., Chamberlin, C., Titov, V., Tang, L., & Bernard, E. N. (2013). Modeling of the 2011 Japan tsunami—Lessons for near-field forecast. *Pure and Applied Geophysics*, *170*(6–8), 1309–1331. <https://doi.org/10.1007/s00024-012-0519-z>.

(Received January 31, 2017, revised December 27, 2017, accepted January 4, 2018)